May 2, 2000

# Antenna control systems: From PI to $H_\infty$

Wodek Gawronski

Jet Propulsion Laboratory
California Institute of Technology
Communications Ground Systems Section
M.S. 238-528
Pasadena, CA 91109
wodek.k.gawronski@ jpl.nasa.gov

## 1. Abstract

Newly designed NASA Deep Space Network antennas are retrofitted for high frequency spacecraft communication, which require high pointing precision. Also, physical dimensions of antennas increase, making the precise pointing task challenging. Many factors contribute to the pointing error budget (e.g. thermal deformations of the structure, gravity distortions, accuracy of the encoder mounting, or wind gust forces acting on antenna structure). In this paper we will discuss the pointing accuracy contributed by the control system. These errors have their sources in the antenna inertia and flexibility, and in wind disturbances acting on the antenna structure. The errors depend on the quality of the antenna drives (hardware), and on the implemented control algorithm (software). We assume that the hardware is not subject to modification. In this way the pointing improvements will depend solely on the control algorithm.

This paper describes three control algorithms: PI (proportional-and-integral), LQG (linear-quadratic-Gaussian) and $H_\infty$ - as applied to antenna tracking. It specifies their basic properties, performances, tracking precision, and limitations. It shows that significant improvement in tracking precision can be achieved by selection of a proper control algorithm. It also shows that further improvements in tracking precision would require concurrent modifications of control algorithm and of antenna drive.

## 2. Introduction

The NASA Deep Space Network (DSN) antennas retrofitted for Ka-band (32 GHz) spacecraft communication require tracking precision of 2 arcsec. This is a challenging requirement for an antenna control engineer. At the same time, the size of antennas increases in order to receive ever-weaker RF signals. This makes the pointing improvement even more challenging.

The purpose of this paper is to describe the development of the antenna control algorithms, from the simplest to the most advanced, to explain their properties, and to analyze their pointing performance, including the performance limits. The paper is based predominantly on the author experience at the DSN antennas, both analytical and from field-testing. The control systems of the NASA DSN antennas have been recently upgraded to improve their tracking precision. The simple proportional and integral (PI) controllers were replaced with the linear-quadratic-Gaussian (LQG) controllers that track with higher precision, see Refs. [1-3]. On the other hand, $H_\infty$ controllers, known to be the most advanced, are considered to be implemented in the antenna servo system, as discussed in Refs. [4,5].

## 3. Antenna under test

The DSS26 antenna of the Deep Space Network is investigated. Shown in Fig.1, this antenna has a 34-meter dish, and is located at the Deep Space Communication Complex at Goldstone, CA. The antenna can rotate with respect to the azimuth (or vertical) axis and elevation (or horizontal) axis. It is driven with electrical DC motors. Its control system was recently upgraded to improve its tracking accuracy.

The open-loop antenna model includes the structure and the drives (motors, gearboxes and amplifiers). It is driven by the rate input signal $u$ [deg/s], see Fig.2a, while the encoder reading $y$ [deg] is the output. Wind disturbance is denoted $w$. In this model wind gusts are additive disturbances to the control signal. The state-space model of the antenna was obtained from the field test data. The antenna was excited with a white noise, sampling time of 0.025s, and the encoder response was recorded. The system identification procedure was used to derive the state-space model from the recorded input and output data. The magnitude and phase of the transfer functions of this model are shown in Fig.3. They consist of an integral part (or rigid body part) that dominates lower frequencies (below 1 Hz), and is characterized with the magnitude slope of -20 dB/dec and with phase of –90 deg. In higher frequencies - above 1 Hz - they consist of the flexible deformations characterized by resonant peaks, and phase shifts of 180 deg at each peak. The validity of these models was checked with the closed-loop pointing simulations and field-test data. The simulation and test results showed significant coincidence, assuring that the analysis results presented below are not far from the real system performance. Note also that EL and AZ models are similar, therefore, in order to save space, we will, from now on, consider AZ model only.

The block diagram of the closed loop system is shown in Fig.2b. It consists of the antenna and the controller. The controller is a computer software that drives the antenna depending on the current antenna position and on the commanded position. The controller has two inputs: the encoder position $y$, and the commanded position (or shorter: command) $r$ [deg]. The controller output is the rate $u_c$ [deg/s] that drives the antenna. In the following we consider PI, LQG and $H_\infty$ controllers.

The antenna motions in AZ and EL axis are independent, therefore the system in Fig.2 a,b represents either AZ or EL control system.

## 4. Performance criteria and design goals

In the analysis below the controller performance is evaluated using the following criteria, and the controller design is guided by the following goals:

- settling time and overshoot of a step response. They are illustrated in Fig.4a. Settling time is defined as the time at which the antenna encoder output remains within 3% threshold of the nominal value of the step command. A 15 s settling time due to a unit step command is illustrated in Fig.4a. Overshoot (in percent) is the relative difference between the maximal encoder output and the commanded step with respect to the value of the commanded step. In Fig.4a the overshoot is 18%. The settling time indicates how fast antenna reacts to the command, and how large is the bandwidth. The goal is to make the settling time minimal.
- Amplitude and settling time of a disturbance step. Wind disturbance in a form of rapid (stepwise) action is suppressed by the controller counteraction. The time required suppressing it, and amplitude of antenna movement do to wind disturbance are measures of the controller performance (the smaller the amplitude and reaction time, the better is the controller). The goal is to minimize the amplitude and the reaction time.
- Bandwidth of the closed loop transfer function. It is illustrated in Fig.4b. Bandwidth is the frequency at which the magnitude drops 3 dB, or to 70.7% below its zero dB level. This is illustrated in Fig.4b, where the bandwidth is 0.14 Hz. The wider bandwidth, the faster and more precise is the antenna. Thus the goal is to maximize the bandwidth.
- Magnitude of the disturbance transfer function. The lower is the magnitude, the better are wind disturbance rejection properties of the controller. The goal is to minimize the magnitude.
- Steady state error in rate offsets. This represents a constant rate lagging, and the error shall be zero in this case.
- Root-mean-square servo error in 10 m/s wind gusts. Wind gust simulations were used to compare the servo performance in wind. The goal is to minimize the error in wind gusts.
- Phase and gain stability margins. Note that *gain crossover* is the frequency at which the open-loop magnitude first reaches the value of unity, and *phase crossover* is the frequency at which the open-loop phase angle first reaches the value of −180 deg. Thus, *gain margin* is the factor by which the open-loop magnitude must be multiplied

to destabilize the system, and *phase margin* is the number of degrees of delay to destabilize the system. The gain and phase margins are the measure of the stability robustness. They show how much the system gain can be changed to destabilize the closed-loop system, and how much signal delay the closed-loop system can tolerate.

Listed above controller design goals are interdependent, for example, settling time and bandwidth, or amplitude of the disturbance step response and wind rms error. In order to minimize them, a weight of importance shall be prescribed to each goal. However, finding the weighting is not an obvious task, and weights are often selected based on the designer previous experience.

## 5. PI controller

Nowadays PI controllers are seldom used to control large antennas, since they cannot meet the stringent pointing requirements. They are commonly used to control antenna's subsystems, such as subreflectors. We shortly outline the performance of a PI controller. The structure of this controller is shown in Fig.5. The command and the encoder signals are compared, and the result is the servo error $e$, $e=r-y$. The servo error is integrated, obtaining the integral of the error, $e_i$. The controller output, $u_c$, is a combination of the servo error multiplied by the gain $k_p$, (called proportional gain), and the integral of the error multiplied by the gain $k_i$ (called integral gain).

In order to understand the PI controller action consider first a proportional controller, assuming the integral gain zero, $k_i=0$ and the proportional gain $k_p=0.5$. The response of the closed loop system to 10 mdeg step command is shown in Fig.6a. This response has no overshoot, and 7 s settling time. The response to the 10 mdeg/s rate offset in Fig.6b has constant servo error (called lagging) of 20 mdeg. It is desirable to have zero lagging, and lagging reduction can be achieved by increased proportional gain. Indeed, increasing the gain to 1.6 produces smaller lagging (6 mdeg), but the system is almost unstable, see step response in Fig.6a.

On the other hand, introducing an integral gain can eliminate the lagging. Using the proportional gain $k_p=0.5$ and the integral gain, $k_i=0.1$ the antenna response to the 10 mdeg/s rate offset was simulated and is shown in Fig.7. The rate-offset response has zero steady-state error, due to the action of the integral part of the controller (for non-zero steady-state error the integral error would grow indefinitely).

Other performance criteria were verified as well. The antenna response to 10 mdeg step command and to 10 mdeg disturbance step are shown in Figs.8a and 8b. The antenna response to 10 mdeg step command exhibits overshoot of 18%, and settling time of 15 s. The settling time is excessive. The disturbance step response is slow and has large amplitude.

The magnitude of transfer function (from the command to the encoder), and the disturbance transfer function (from the wind disturbance to the encoder) are shown in

Figs.8c and 8d, respectively. The first transfer function show the bandwidth of 0.1 Hz and a strong resonance peak of 2 Hz. The bandwidth is narrow. The disturbance transfer function tends to zero for low frequencies, and also has strong resonance peak at 2 Hz. The magnitude of the disturbance transfer function is too high to produce good disturbance rejection properties.

The stability margins are shown in Fig.9a. The margins are large, indicating that this servo system is robust: the gain margin is 10.3 dB and the phase margin is 69 deg, see Table 1. However, the servo error in 10 m/s wind gusts is quite large: 5.8 arcsec, see Table 2.

The above analysis indicates that the PI servo performance is not satisfactory, and needs improvement. We already noticed that increased proportional gain improves tracking properties (faster step response, and increased bandwidth), and reduces servo error in wind. Unfortunately, the gain increase is limited since it leads to instability of the closed loop system. Thus, the PI controller performance is limited, and it has to be replaced.

## 6. LQG controller

As said before, the bandwidth, speed of the system response, and the disturbance suppression of the PI controller improve with the increase of the controller proportional gain. The gain increase is limited, since excessive gains excite antenna vibrations. However, if the vibrations could be controlled during the gain increase the performance can be improved improved. The basic obstacle in the vibration control is the lack of the vibration sensors at the antenna. Encoder is the only sensor available. However, antenna vibrations are included in the encoder responses (see, for example, the vibrations visible in the step response, Fig.6). The information on antenna vibrations included in the antenna encoder can be recovered by using antenna state estimator. The estimator is the antenna analytical model driven by the same input as the antenna itself (rate input $u$), and by the estimation error $\varepsilon$ (a difference between the actual encoder reading and the estimated encoder reading), see Fig.10. The estimation error is amplified with the estimator gain $k_e$ to correct for transient dynamics. The output of the estimator are the antenna states that include the estimated encoder reading (noise free) and the estimated antenna states ($x_f$) of the flexible deformations of the antenna structure. Thus the estimator supplies the missing measurements of antenna vibrations. Now the controller output is a sum of the familiar PI controller outputs and the flexible mode controller output (obtained as the estimated flexible states amplified by the gain $k_f$). The latter output cancels antenna vibrations.

In this configuration the increased proportional and integral gains do not de-stabilize the closed-loop system, since the flexible-mode controller keeps the flexible antenna vibrations under control. With this ability, one can expect an unlimited increase of the gains without de-stabilization the closed loop system. Indeed, analytically, one can obtain outstanding performance, such as almost immediate response of the antenna to a step

command. However, such a system although stable is not robust – small variations of parameters can de-stabilize this nicely performing system. The robustness, measured as gain and phase margin, will be evaluated for the LQG controller.

The performance of the LQG controller is illustrated with the response to 10 mdeg step command (Fig.11a), response to 10 mdeg disturbance step (Fig.11b), response to 10 mdeg/s rate-offset (Fig.8), and transfer functions: from command to encoder (Fig.11c), and from disturbance to encoder (Fig.11d). The step response has small settling time of 2 s, disturbance step response – low overshoot (3 mdeg) of short duration (2 s), rate offset show zero steady-state error (zero lagging), the command transfer function has wide bandwidth of 2 Hz, and the disturbance transfer function has small magnitude (below 1). The stability margins are shown in Fig.9b. The gain margin is 7.1 dB and phase margin is 45 deg, see Table 1. These are large enough margins to consider this particular LQG controller robust ("better" controllers, with shorter response times, and disturbance rejection properties had small margins). The servo error in 10 m/s wind gusts is small: 0.10 arcsec, see Table 2. These parameters show that the LQG controller is of an order better than the PI controller. The question appears: Can one go further? The possibility is the $H_\infty$ controller.

## 7. $H_\infty$ Controller

$H_\infty$ controller is known to outperform LQG controllers in many applications. The structure an $H_\infty$ controller is similar to the LQG controller, although its parameters are obtained from a different algorithm that minimizes the system $H_\infty$ norm (in case of single-input-single-output system, the system $H_\infty$ norm is the maximal magnitude of its transfer function).

The $H_\infty$ controller was designed using weighted disturbance input. A filter of the Davenport wind spectrum profile was used as a weighting factor. The performance of the antenna was evaluated as a weighted servo error and its integral.

Separate controllers were designed for the AZ and EL axes, and the results are summarized in the Table 1 for AZ and EL axes. The table shows very small servo error in the 10 km/h wind gusts.

Additional results for AZ axis are shown and Fig.12. The figures show very small settling time (1.2 s), small overshoot (less than 10 %), wide bandwidth (over 2 Hz). These features significantly exceed LQG controller performance. The response to the 10 mdeg/s rate offset is shown in Fig.8. It has zero steady-state error and short settling time (below 1 s). Disturbance transfer function (Fig.12d) has very low magnitude, below 0.1. The servo error in 10 m/s wind gusts is small: 0.08 arcsec, see Table 2. The stability margins are shown in Fig.9c. The gain margin is 7.9 dB and the phase margin is 42 deg, as shown in Table 2. They are similar to the LQG controller, and show controller robustness.

In spite of these outstanding features, our simulations and also measurements show that the $H_\infty$ controllers cannot be implemented directly, i.e. without modifications of the existing antenna drives (motors and gearboxes). The main obstacle is the motor load, expressed as the acceleration limit imposed on the input signal $u$ that drives the antenna. The limit is imposed to prevent overloading of the motors. For the DSS26 antenna the acceleration limits are $\pm 0.4$ deg/s$^2$.

For the $H_\infty$ controller the acceleration during 10 mdeg step offset is shown in Fig.13. The acceleration reaches the value of 20 deg/s$^2$, much higher than the limit. The acceleration limiter reduces these values to $\pm 0.4$ deg/s$^2$, but this reduction produces non-linear operation that de-stabilizes the system (the estimator is linear, and does not reproduce the acceleration limits).

One way to avoid excessive accelerations is to implement a command pre-processor, as in Ref.[7]. The preprocessor is a computer software that modifies antenna commands such that they never exceed the rate and acceleration limits. It commands the antenna with the maximal rate and/or acceleration if the rate and/or acceleration limits of the command are exceeded, and commands it with an unmodified command if the limits are not exceeded. This approach worked for LQG controllers and for $H_\infty$ controllers in no-wind condition. However, in a windy weather the antenna is moved not only by the command, but also by the wind gusts. In this scenario the input $u$ is a combination of the command and of the fed back wind disturbance. Although command, due to preprocessor, is below the acceleration limits, the fed back signal, due to strong reaction of the $H_\infty$ controller to wind gusts, exceeds the limits, and destabilizes the system. This behavior indicates that the improvement of the $H_\infty$ controller performance is tied to the relaxation of the acceleration limits imposed on the antenna drives. The acceleration limits, imposed to prevent excessive loads at the motor, can be relaxed if more powerful motor replaces the existing one. Thus the further improvements of the antenna performance beyond the presented above LQG performance requires not only modifications of the control software (control algorithm) but also requires hardware modifications (more powerful motors and stronger gearboxes).

## 8. Conclusions

We showed that the LQG controller significantly outperformed the PI controller in terms of faster reaction to a command, wider bandwidth, better pointing precision, and smaller pointing error in wind gusts. We also showed that implementation of LQG controller algorithm requires software modification only. Further improvements, if necessary, can be achieved by implementing the $H_\infty$ controller. However, this implementation, needs more powerful motors to drive the antenna, so that their acceleration limits are less restrictive and do not interfere with the servo algorithm. Thus the upgrade to $H_\infty$ controller requires not only software modifications but also hardware upgrade.

## 9. Acknowledgements

The research described in this paper was carried out by the Jet Propulsion Laboratory, California Institute of Technology, under a contract with the National Aeronautics and Space Administration.

## 10. References


1. W. Gawronski, C. S. Racho, and J. A. Mellstrom "Linear Quadratic Gaussian and Feedforward Controllers for the DSS-13 Antenna," *TDA Progress Report,* No. 42-118, 1994, http://tmo.jpl.nasa.gov/tmo/progress_report/42-118/118D.pdf
2. W. Gawronski, and J.A. Mellstrom, "Control and Dynamics of the Deep Space Network Antennas," in: *Control and Dynamics Systems*, ed. C.T. Leondes, vol. 63, Academic Press, San Diego, CA, 1994, pp. 289-412.
3. W. Gawronski, C. Racho, and J.A. Mellstrom, "Application of the LQG and Feedforward Controllers for the DSN Antennas," *IEEE Trans. on Control Systems Technology*, vol.3, 1995.
4. W. Gawronski, "An $H_\infty$ Controller With Wind Disturbance Rejection Properties for the DSS-13 Antenna," TDA PR 42-127, July-September 1996, pp. 1-15, November 15, 1996 http://tmo.jpl.nasa.gov/tmo/progress_report/42-127/127G.pdf.
5. W. Gawronski, *Dynamics and Control of Structures: A Modal Approach*, Springer-Verlag, New York, 1998.
6. W. Gawronski, "Wind Gust Models Derived From Field Data," *TDA Progress Report,* No. 42-123, 1995, http://tmo.jpl.nasa.gov/tmo/progress_report/42-123/123G.pdf
7. W. Gawronski, "Command Preprocessor for the Beam-Waveguide Antennas," TMO PR 42-136, October-December 1998, pp. 1-10, February 15, 1999, http://tmo.jpl.nasa.gov/tmo/progress_report/42-136/136A.pdf.

**Table 1.** Rms servo error in 10 m/s wind gusts

| Controller | Servo error (arcsec) |
|---|---|
| PI (AZ) | 1.8 # |
| PI (EL) | 5.8# |
| LQG (AZ) | 0.10 |
| LQG (EL) | 0.39 |
| $H_\infty$ (AZ) | 0.08 |
| $H_\infty$ (EL) | 0.18 |

# from measurements, see Ref.[4].

**Table 2.** Stability margins

| Controller | Gain margin (dB) | Phase margin (deg) |
|---|---|---|
| PI (AZ) | 10.3 | 69 |
| PI (EL) | 6.2 | 69 |
| LQG (AZ) | 7.1 | 45 |
| LQG (EL) | 4.8 | 38 |
| $H_\infty$ (AZ) | 7.9 | 42 |
| $H_\infty$ (EL) | 5.1 | 33 |

FIGURES:

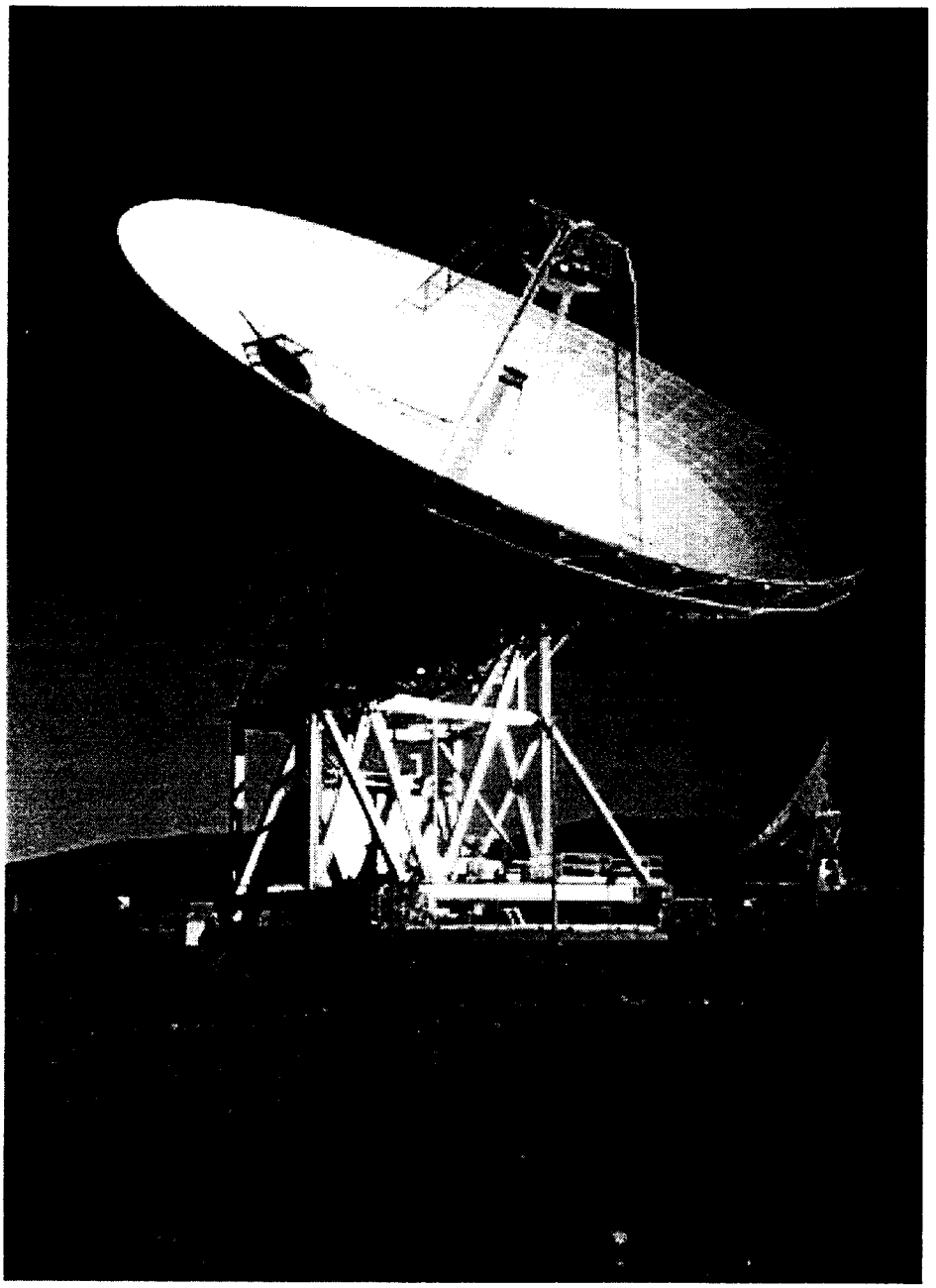

Figure 1.

(a)

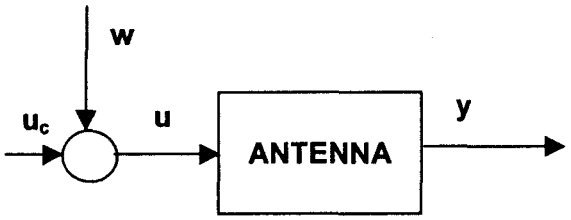
w
$u_c$
u
ANTENNA
y

(b)

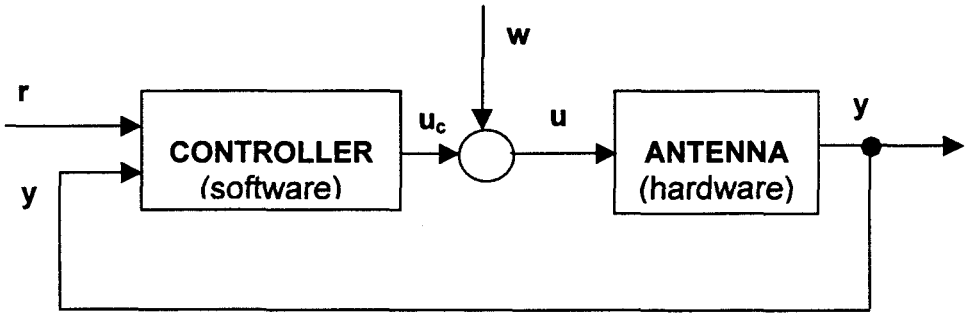
w
r
CONTROLLER
(software)
$u_c$
u
ANTENNA
(hardware)
y
y

**Figure 2.**

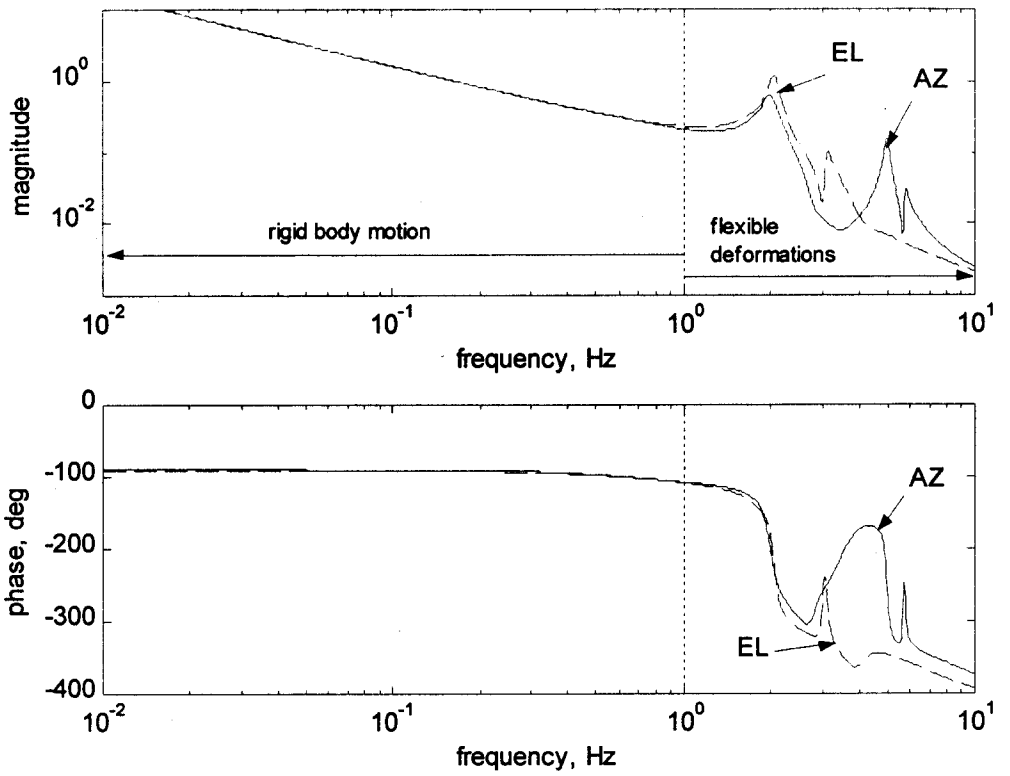
magnitude
$10^0$
$10^{-2}$
EL
AZ
rigid body motion
flexible
deformations
$10^{-2}$
$10^{-1}$
$10^0$
$10^1$
frequency, Hz
phase, deg
0
-100
-200
-300
-400
AZ
EL
$10^{-2}$
$10^{-1}$
$10^0$
$10^1$
frequency, Hz

**Figure 3.**

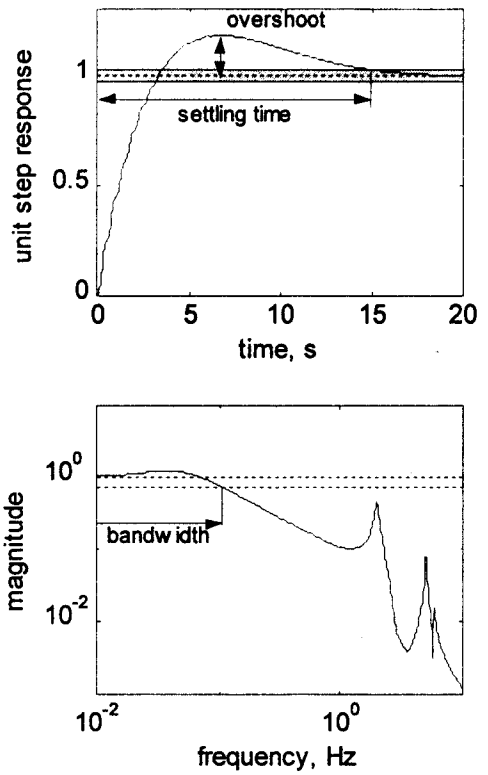
overshoot
settling time
unit step response
1
0.5
0
0
5
10
15
20
time, s
magnitude
$10^0$
$10^{-2}$
bandwidth
$10^{-2}$
$10^0$
frequency, Hz

**Figure 4.**

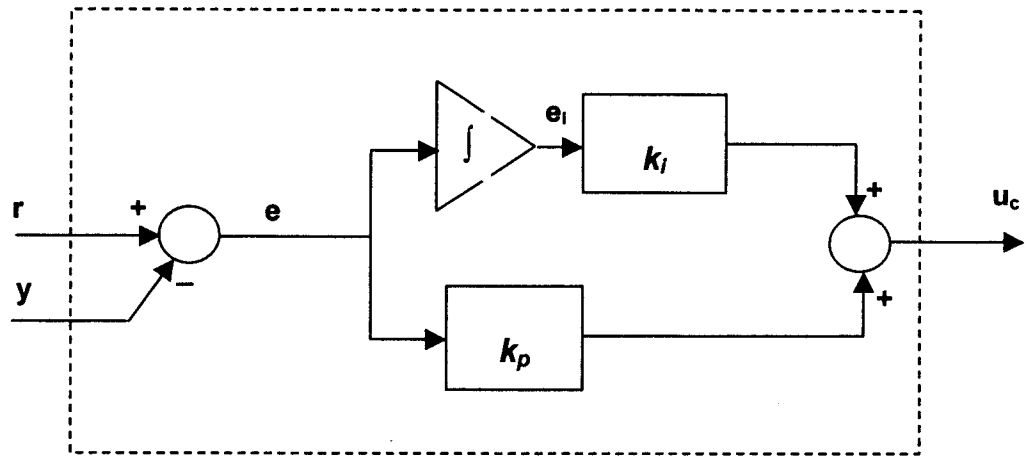


**Figure 5.**

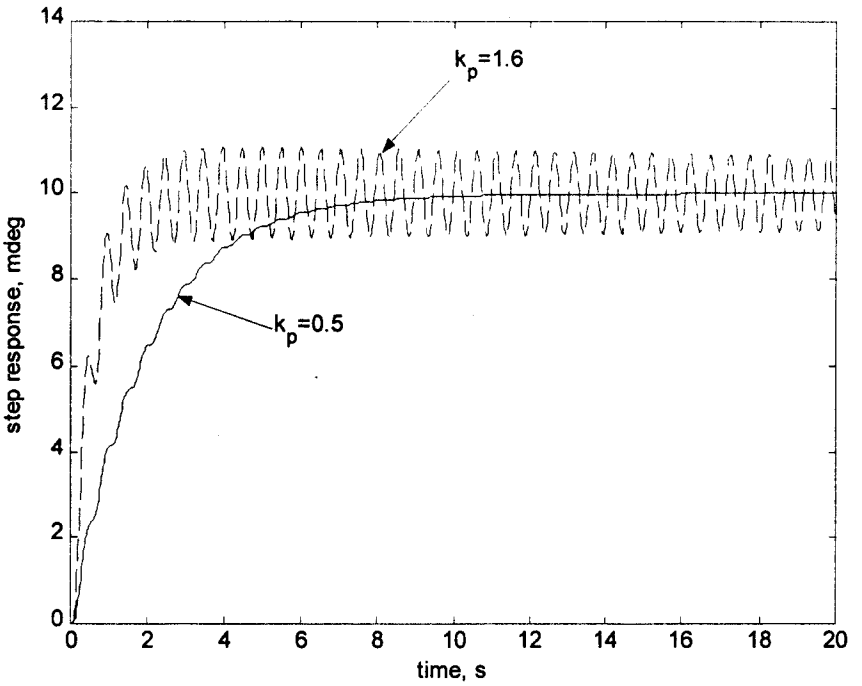


**Figure 6a.**

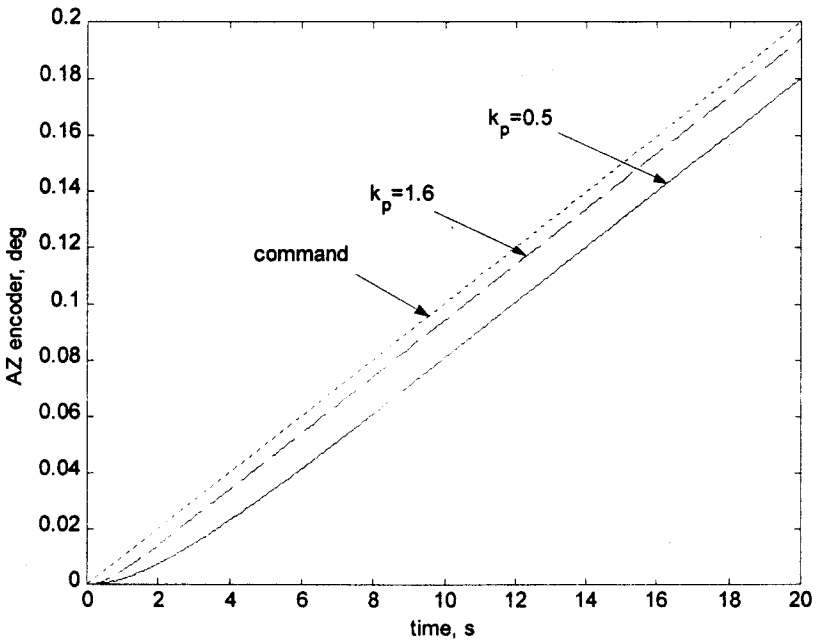


**Figure 6b.**

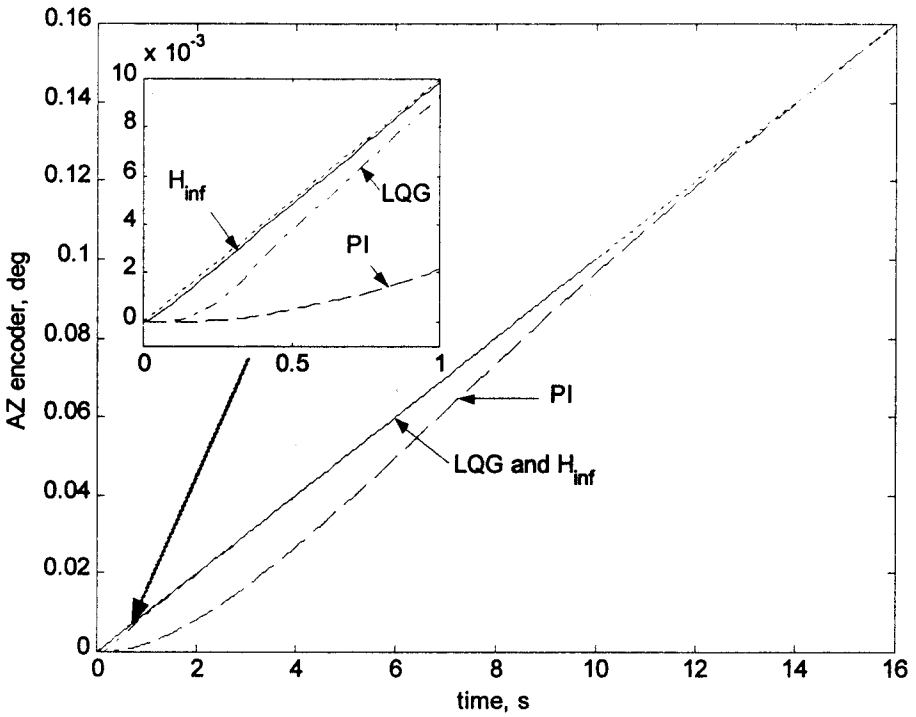


**Figure 7.**

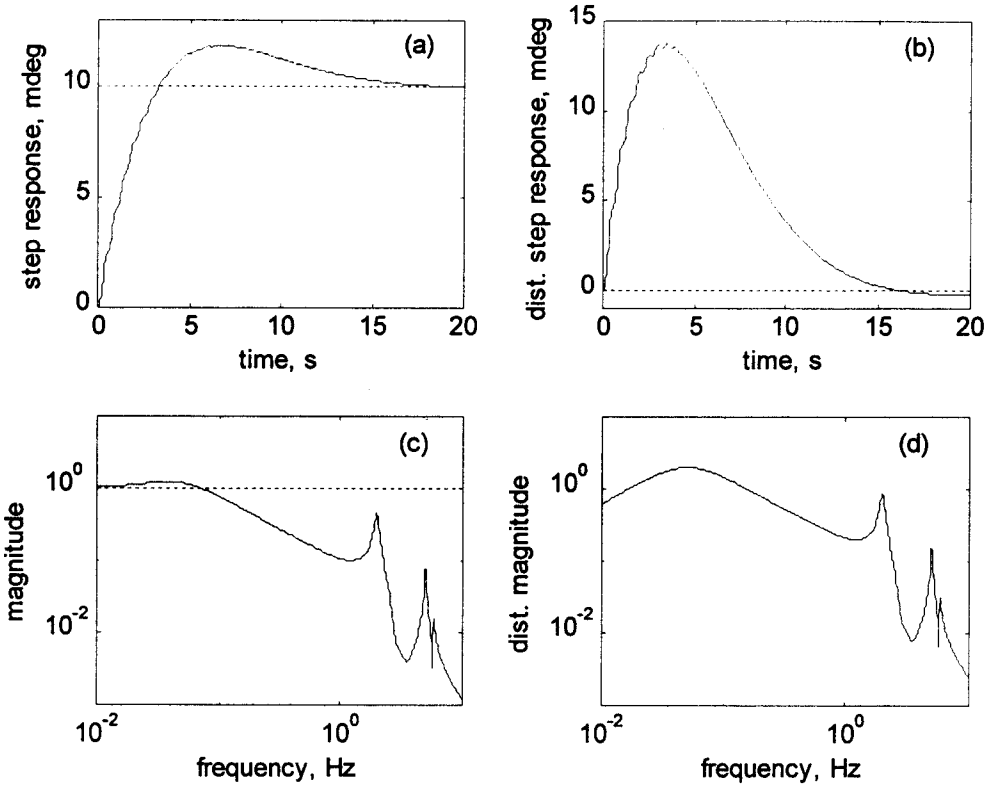
(a)
step response, mdeg
10
5
0
0
5
10
15
20
time, s
(b)
dist. step response, mdeg
15
10
5
0
0
5
10
15
20
time, s
(c)
magnitude
$10^0$
$10^{-2}$
$10^{-2}$
$10^0$
frequency, Hz
(d)
dist. magnitude
$10^0$
$10^{-2}$
$10^{-2}$
$10^0$
frequency, Hz

**Figure 8.**

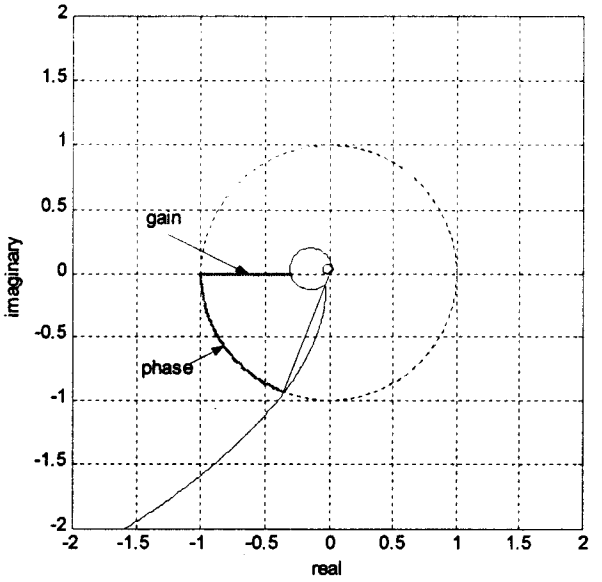
gain
phase
imaginary
real
2
1.5
1
0.5
0
-0.5
-1
-1.5
-2

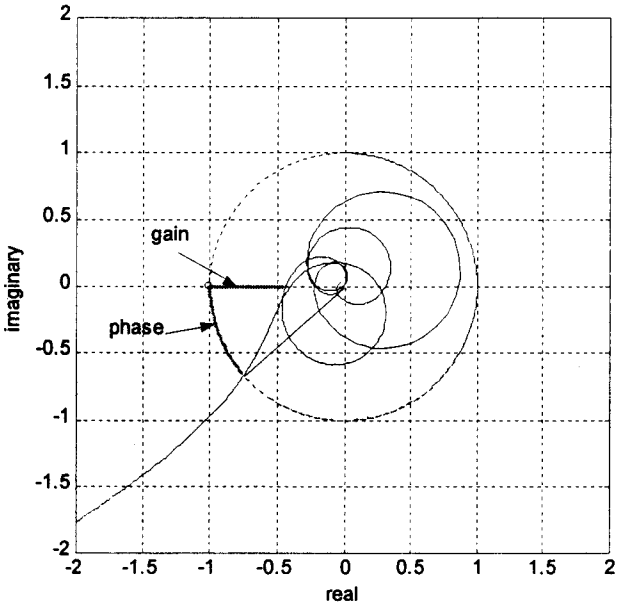
gain
phase
imaginary
real
2
1.5
1
0.5
0
-0.5
-1
-1.5
-2

**Figure 9 a,b.**

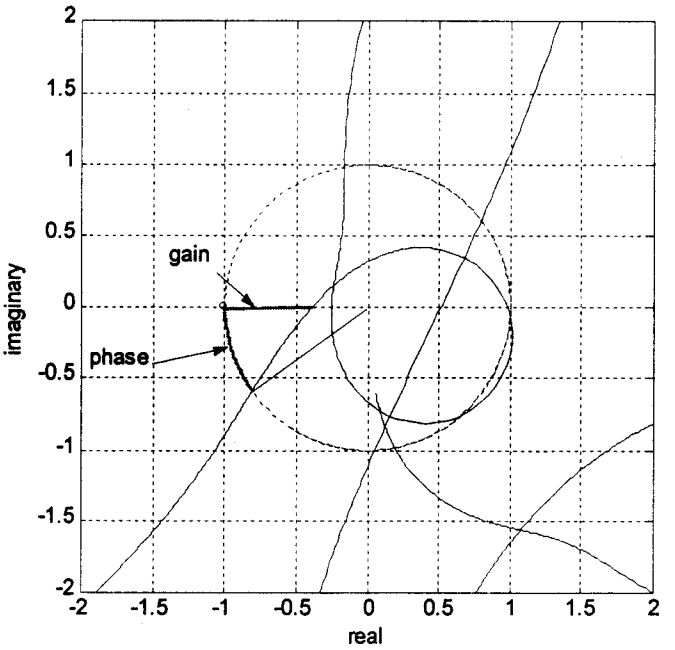


**Figure 9 c.**

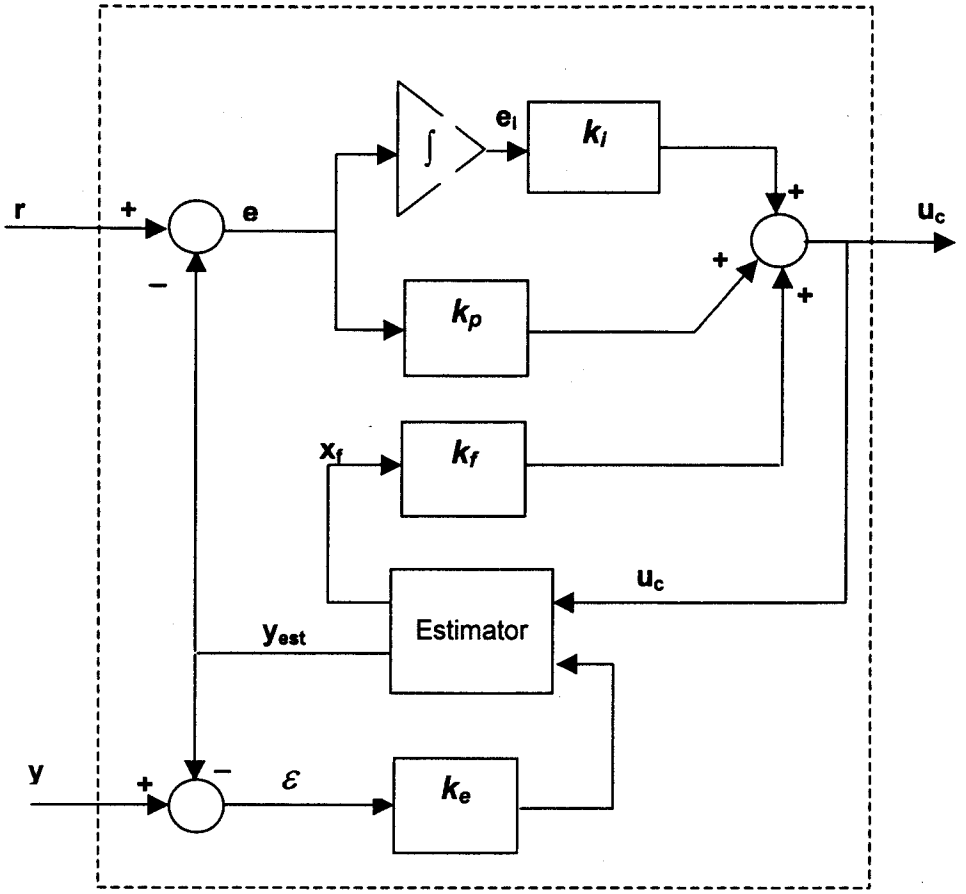


**Figure 10.**

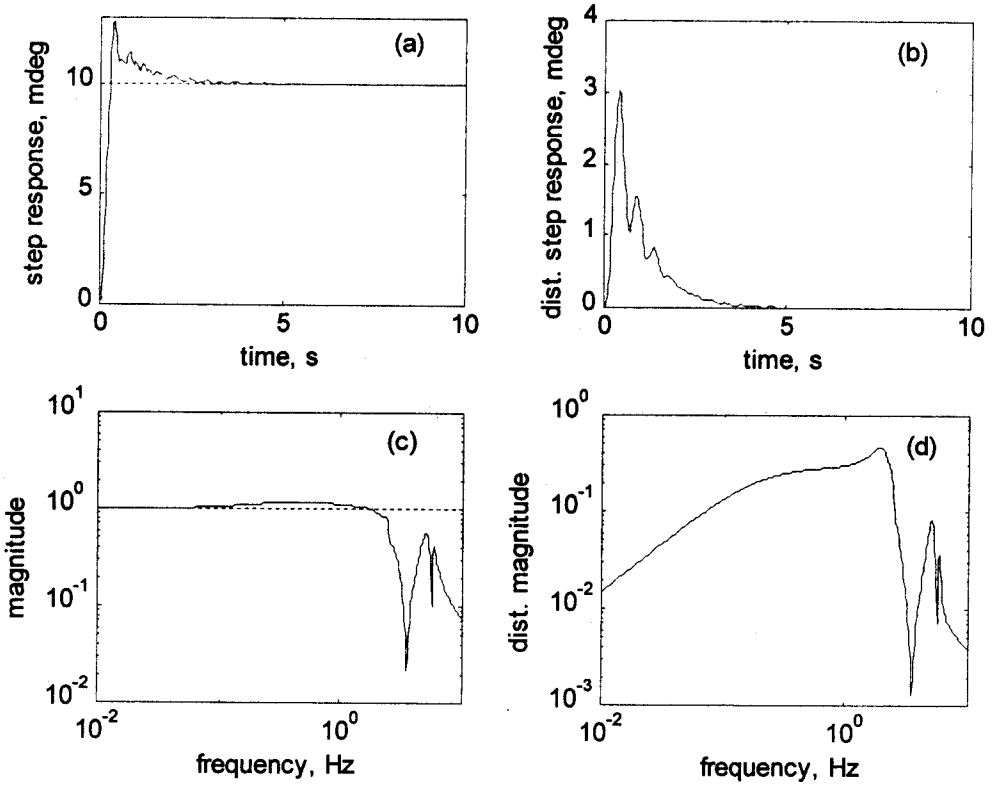
(a)
step response, mdeg
10
5
0
0
5
10
time, s
(b)
dist. step response, mdeg
4
3
2
1
0
0
5
10
time, s
(c)
magnitude
$10^1$
$10^0$
$10^{-1}$
$10^{-2}$
$10^{-2}$
$10^0$
frequency, Hz
(d)
dist. magnitude
$10^0$
$10^{-1}$
$10^{-2}$
$10^{-3}$
$10^{-2}$
$10^0$
frequency, Hz

**Figure 11.**

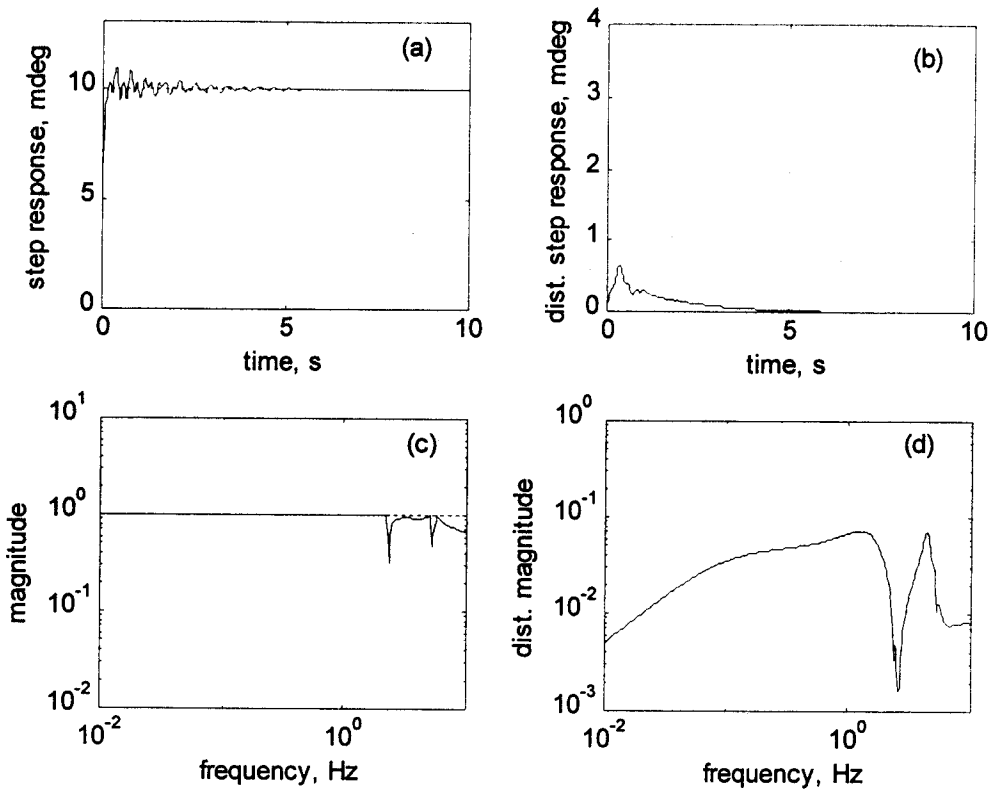
(a)
step response, mdeg
10
5
0
0
5
10
time, s
(b)
dist. step response, mdeg
4
3
2
1
0
0
5
10
time, s
(c)
magnitude
$10^{1}$
$10^{0}$
$10^{-1}$
$10^{-2}$
$10^{-2}$
$10^{0}$
frequency, Hz
(d)
dist. magnitude
$10^{0}$
$10^{-1}$
$10^{-2}$
$10^{-3}$
$10^{-2}$
$10^{0}$
frequency, Hz

**Figure 12.**

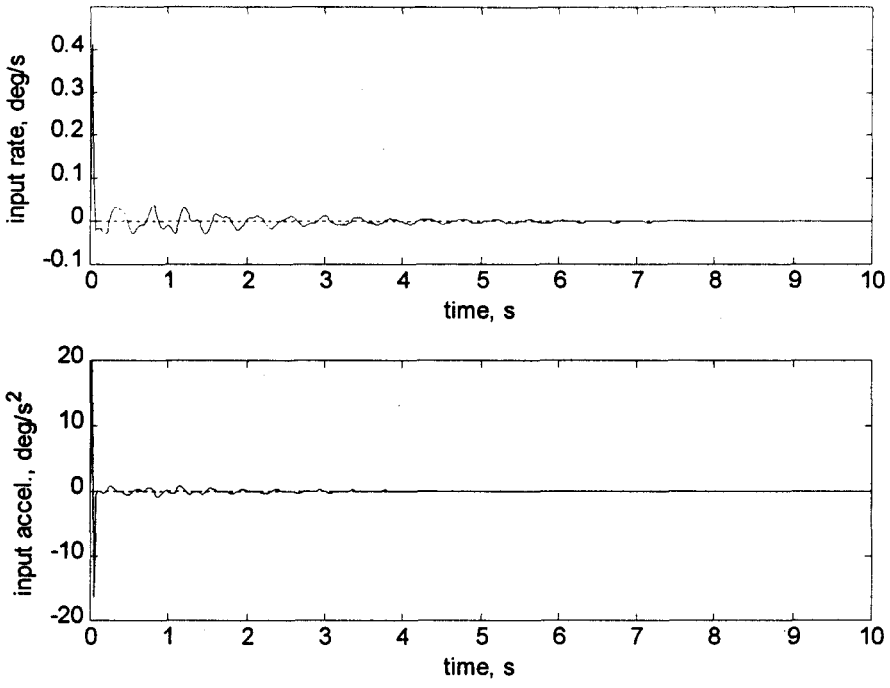
input rate, deg/s
0.4
0.3
0.2
0.1
0
-0.1
0 1 2 3 4 5 6 7 8 9 10
time, s
input accel., deg/s2
20
10
0
-10
-20
0 1 2 3 4 5 6 7 8 9 10
time, s

**Figure 13.**